Coaggregation of B−C and D−C Diblock Copolymers with H-Bonding C Blocks in Block-Selective Solvents

Xiaohu Yan, Guojun Liu,* and Jiwen Hu

Department of Chemistry, Queen's University, 90 Bader Lane, Kingston, Ontario, Canada K7L 3N6

C. Grant Willson

Department of Chemical Engineering, University of Texas at Austin, Austin, Texas 78712-1167

Received November 14, 2005; Revised Manuscript Received January 12, 2006

ABSTRACT: Studied by dynamic light scattering (DLS) and transmission electron microscopy (TEM) is the coaggregation of poly(*tert*-butyl acrylate)-*block*-poly(2-cinnamoyloxyethyl methacrylate), PtBA−PCEMA, and polystyrene-*block*-poly(2-cinnamoyloxyethyl methacrylate), PS−PCEMA, in mixtures of chloroform and hexane, where hexane is a precipitant for PCEMA and PS but a good solvent for PtBA. To ensure coaggregation, the PCEMA blocks in the different diblocks were tagged by the H-bonding DNA base pair thymine and adenine. Coaggregation of the associating diblocks resulted in interesting block copolymer aggregation behavior and morphologies.

I. Introduction

Aggregation of diblock copolymers in block-selective solvents yields nanoparticles with shapes ranging from spheres[1,2] to cylinders,[3−5] tubes,[6−10] vesicles,[4,5,11−14] donuts,[5,15,16] and many others.[17] The shape diversity of such aggregates may help their applications in nanofabrication,[18−20] lithography,[21−23] cell culturing,[24,25] drug delivery,[26,27] etc. Many more morphologies are expected of aggregates of B−C−D triblock copolymers. Despite this, there have been not many reports on morphologies of micelles of B−C−D triblock copolymers. One possible reason for this is the difficulty associated with the preparation of well-defined triblock copolymers. Jiang and co-workers[28−30] reported recently on the preparation of "pseudo-graft" copolymers from a homopolymer pair with one bearing a terminal H-bond donor (acceptor) and the other containing H-bond acceptors (donors) along the chain. Such pseudo-graft copolymers formed nanoaggregates in block-selective solvents just like conventional graft copolymers or even diblocks. Jiang's strategy can be extended to the preparation of "pseudo" B−C−D triblocks from two associating diblock copolymers B−C and D−C with H-bonding C blocks. We report in this paper the coaggregation of two such associating diblocks in block-selective solvents either for the B and D blocks or for the B block only. In solvents that solubilize only the B block, we report also a novel space-filling molecular-model-like morphology for the coaggregates formed.

The specific diblock copolymers used in this study are poly(*tert*-butyl acrylate)-*block*-poly{(2-cinnamoyloxyethyl methacrylate)-*ran*-[2-(1′-thyminylacetoxyethyl methacrylate)]}, PtBA−P(CEMA-T), and polystyrene-*block*-poly{(2-cinnamoyloxyethyl methacrylate)-*ran*-[2-(1′-adeninylacetoxyethyl methacrylate)]}, PS−P(CEMA-A). The H-bonding thymine and adenine groups were introduced into the polymers mainly to facilitate the association of the two diblocks in non-H-bonding solvents including chloroform (CF) and hexane (HX). PCEMA was used, on one hand, for its selective staining by OsO_4 and thus its spatial identification in nanoaggregates by transmission electron microscopy (TEM) and, on the other hand, for its photo-cross-linkability. Photo-cross-linking allowed the structural locking of the aggregates formed. Structurally stable aggregates could then be treated chemically for PtBA hydrolysis to poly(acrylic acid) or PAA. PAA, unlike PtBA, could be selectively stained, e.g., by uranyl acetate [$UO_2(Ac)_2$], and thus allowed the back tracking of the spatial location of PtBA in a nanoaggregate. To prepare the nanoaggregates, we started by equilibrating the associating diblocks in CF overnight. Coaggregates were produced by adding HX, a selective solvent for PtBA. Depending on the hexane content, the solvent mixtures could be selectively good for both PtBA and PS or for PtBA only.

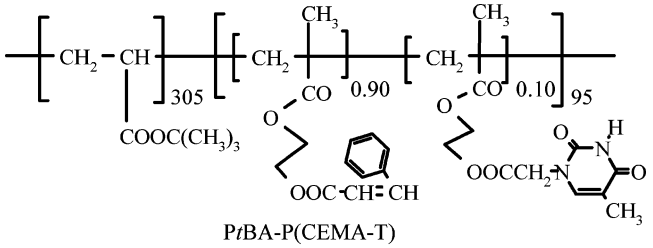

II. Experimental Section

Reagents. Chloroform (99.9%), hexane (99.9%), methylene chloride (95.5%), *N*,*N*-dimethylformamide (DMF, 99.9%), and tetrahydrofuran were purchased from Fisher Scientific and were used as received. Trifluoroacetic acid (99%) and triethylsilane (99%) were purchased from Aldrich.

Transmission Electron Microscopy. Aggregates prepared in CF/HX were aspirated using a home-built device[31] onto carbon-coated copper grids and stained by OsO_4 vapor for 2 h before TEM observation. Aggregate samples after PCEMA cross-linking and PtBA hydrolysis were aspirated from DMF. After DMF evaporation,

* Corresponding author. E-mail: gliu@chem.queensu.ca.

10.1021/ma052435i CCC: $33.50
Published on Web 02/11/2006

Table 1. Characteristics of the Diblocks Used

sample	SEC M_w/M_n	dn_r/dc (mL/g)	LS M_w (g/mol)	NMR n/m	n_w	T% or A%
PS−P(CEMA-A)	1.19	0.160[a]	8.4×10^4 [a]	6.6	590	13%
PtBA−P(CEMA-T)	1.11	0.114[b]	6.4×10^4 [b]	3.2	305	10%

[a] Measured in DMF. [b] Measured in butanone.

drops of a uranyl acetate solution at 0.05 g/mL were added on the films to stain the PAA groups for 10 min. The excess staining agent was removed by rinsing the grids with methanol droplets several times. All TEM observations were made on a Hitachi 7000 instrument operated at 75 kV.

Dynamic Light Scattering. For DLS analyses of the individual PtBA−P(CEMA-T) and PS−P(CEMA-A) samples, PtBA−P(CEMA-T) and PS−P(CEMA-A) were first solubilized in 1.0 mL of CF at 20.0 and 9.6 mg/mL, respectively. The CF solutions were then carefully dispensed into a quartz light scattering cell with a diameter of 22 mm through a 0.1 μm PTFE filter (Whatman Co.). Further filtered into the cell was HX in aliquots to gradually increase the HX content. After the addition of each aliquot of HX and its quantification by mass change, DLS measurement was performed in 10 min.

Two protocols were used to prepare mixed PtBA−P(CEMA-T) and PS−P(CEMA-A) samples in CF/HX. Regardless of the protocols, PtBA−P(CEMA-T) and PS−P(CEMA-A) at a weight ratio of 1.00/1.00 were first equilibrated in CF at a total polymer concentration of ~5.5 mg/mL for at least 12 h. The diblock mixture solution was then divided among several vials. The amount of CF solution in the vials varied depending on the final HX volume fraction f_{HX} required. For $f_{HX} = 40\%$ and $f_{HX} = 90\%$, the volumes of the CF solution used were 0.70 and 0.30 mL, respectively. The amount of the CF solution used was decreased as f_{HX} increased because we needed only about 2.5 mL of the final solution for DLS and TEM analyses. In protocol 1, a known amount of HX was injected within fractions of a second into a vial under vigorous stirring. In protocol 2, HX was added via a pump at 0.07 mL/min. Thus, the HX addition rate was orders of magnitude faster in protocol 1 than in protocol 2.

After the completion of HX addition, a solution was immediately filtered into a light scattering cell. For samples with $f_{HX} < 60\%$, 0.2 μm filters were used to clarify the samples. Filters with porosity at 0.45 μm were used to clarify the other samples. To construct plots depicting d_h and K_2/K_1^2 variation as a function of f_{HX}, the DLS data were obtained 10 min after HX addition. In the neighborhood of $f_{HX} = 75\%$, we have also obtained d_h variation as a function of time after HX addition.

DLS analyses were performed using a Brookhaven model 9025 instrument equipped with a 632.8 nm He−Ne laser. DLS data were analyzed by the cumulant method[32] to yield sample hydrodynamic diameters d_h and polydispersity K_2/K_1^2.

Density and Viscosity of the Solvent Mixtures. To determine the density ρ_2 of a CF/HX mixture, 1.00 mL of the mixture was pipetted into a vial. Its mass was then measured using an analytical balance. The ρ_2 value was taken as the average from three measurements.

The viscosity η_2 of a solvent mixture was obtained from comparing the flow time of the mixture and that t_1 of CF through a Ubbelohde capillary viscometer at room temperature (22 °C) using

$$\eta_2 = \eta_1\left(\frac{\rho_2 t_2}{\rho_1 t_1}\right) \quad (1)$$

where the viscosity η_1 of CF was taken to be 0.5576 cP as interpolated from the viscosity data of CF at 20 and 25 °C reported in a handbook.[33]

PCEMA Cross-Linking and PtBA Hydrolysis. Aggregates of mixed diblocks were prepared at $f_{HX} = 66\%$ and $f_{HX} = 90\%$ using protocol 1. For PCEMA cross-linking, the aggregate solutions were irradiated by a focused UV beam that had passed through a 270 nm cutoff filter from a 500 W Hg lamp at 20 °C for 2 h. This led to a CEMA double-bond conversion of ~35% as estimated from CEMA absorbance decrease at 274 nm.[34] To hydrolyze PtBA,[35] a sample after PCEMA cross-linking was dried by rotaevaporation and then redispersed in methylene chloride. Trifluoroacetic acid at a volume ratio of 1:3 relative to methylene chloride and triethylsilane at a molar ratio of 3:1 relative to the tBA groups were added. After 2 h, the aggregates were precipitated into diethyl ether and washed by diethyl ether three times to remove the residual acid. The aggregates were redispersed in DMF for TEM study.

III. Results and Discussion

Polymer Characterization. The procedures for the synthesis and characterization of the PtBA−P(CEMA-T) and PS−P(CEMA-A) families of polymers have been recently reported[36] and were thus not repeated in the Experimental Section. For characterization, the size exclusion chromatography (SEC) weight-average molar masses M_w and polydispersity indices M_w/M_n were measured in THF based on PS standards. The specific refractive index increments dn_r/dc and light scattering (LS) or weight-average molar masses M_w were determined in DMF for PS−P(CEMA-A) and in butanone for PtBA−P(CEMA-T), respectively. The ratio n/m of repeat unit numbers for the two blocks of a diblock and the T and A molar content, T% and A%, in the PCEMA blocks were determined from ^{1}H nuclear magnetic resonance (NMR) analysis. Table 1 summarizes the characteristics of the samples used in this study. We have included the weight-average number of repeat units n_w calculated using the LS M_w and NMR n/m values rather than the number-average number of repeat units n_n for PS and PtBA in the table because the SEC M_w/M_n values were inaccurate. Results of Table 1 show that the length of PCEMA blocks of the two diblocks is approximately the same around 90.

H-Bond Formation between the T and A Groups in Chloroform. H-bond formation between A and T or between derivatives of this DNA base pair in chloroform has been firmly established.[37] The binding between the A and T groups of PtBA−P(CEMA-T) and P(hCEMA-A) in CF and their dissociation in DMF have been recently used to produce solvent-dispersible porous nanospheres that recognized P(hCEMA-A) for resorption,[38−40] where P(hCEMA-A) denotes poly(2-hydrocinnamoyloxyethy methacrylate) tagged by A units. The binding between P(CEMA-A) and P(CEMA-T) here leads to PS−P(CEMA-A) and PtBA−P(CEMA-T) chain association. This should be accompanied by a decrease in the system's entropy. Also, this association would take place only if the repulsion between the immiscible PtBA and PS chains was overcome.[36] For these, it is anticipated that the T and A concentration had to be sufficiently high, e.g., T% ≈ A% ≈ 10%, to enable chain association. Our DLS analyses yielded the d_h values of 7.3, 10.1, and 11.9 nm for the PtBA−P(CEMA-T), PS−P(CEMA-A), and a mixture of the two diblocks at wt/wt = 1.00/1.00 in CF, respectively. The fact that the d_h value of the diblock mixture in CF was the largest suggests the association of the PtBA−P(CEMA-T) and PS−P(CEMA-A) chains in CF. Other evidence suggesting this association will become self-evident later as we discuss the various coaggregation phenomena of the diblocks in CF/HX.

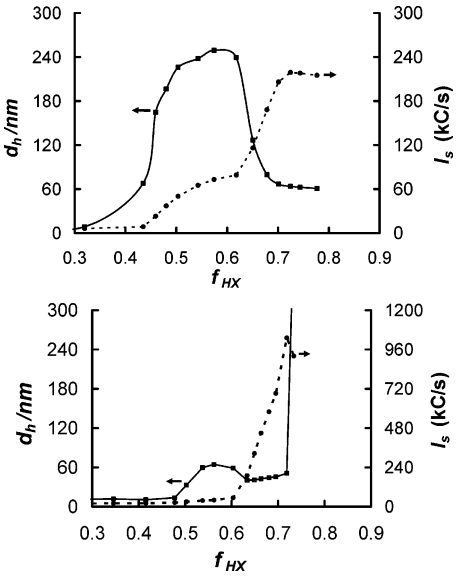

Figure 1. Plot of d_h (■) and I_s (●) variation as a function of f_{HX} for the PtBA−P(CEMA-T), top panel, and PS−P(CEMA-A), bottom panel, samples in CF/HX.

Viscosities of CF/HX Mixtures at 22 °C. Determination of d_h for the block copolymer samples in different CF/HX mixtures at room temperature from DLS required knowledge of viscosity η_2 of the solvent mixtures. We determined experimentally η_2 of nine mixtures and found that the data were best fitted by a quadratic equation:

$$\eta_2 = 0.3147 + 0.1991 f_{CF} + 0.0429 f_{CF}^{\ 2} \quad \text{cP} \qquad (2)$$

The use of eq 2 allowed η_2 calculation at any other f_{CF} values, where f_{CF} denotes the CF volume fraction.

DLS Study of Individual PtBA−P(CEMA-T) and PS−P(CEMA-A) Samples. HX is a precipitant for both PCEMA and PS. To know which of the PCEMA and PS blocks collapsed from the solvent phase first, we examined the aggregation behavior by DLS of the individual PtBA−P(CEMA-T) and PS−P(CEMA-A) samples in CF/HX with different f_{HX}.

Figure 1 compares the variation trends in the d_h values of the two diblocks in different CF/HX mixtures. PtBA−P(CEMA-T) began to form aggregates at $f_{HX} \approx 45\%$. The d_h value of the aggregates peaked at ~240 nm at $f_{HX} = 57\%$ before it began to decrease. The size of the aggregates stabilized at ~60 nm at $f_{HX} > 70\%$, suggesting formation of spherical micelles.

The same d_h value variation trend was noticed of the PS−P(CEMA-A) sample before $f_{HX} \approx 72\%$. PS−P(CEMA-A) aggregates started to form at $f_{HX} \approx 50\%$. The d_h value peaked at ~65 nm at $f_{HX} \approx 56\%$. It then decreased and stabilized at ~45 nm, suggesting formation of also spherical micelles. At $f_{HX} = 73.3\%$, we noticed visually that the sample was getting more cloudy with time and eventually precipitated from the solution in 0.5 h.

The fact that the PtBA−P(CEMA-T) and PS−P(CEMA-A) samples had a similar d_h value variation pattern before $f_{HX} \approx 72\%$ suggests that the P(CEMA-T) and P(CEMA-A) blocks collapsed from the solvent phase before the PS block. The PtBA−P(CEMA-T) sample formed stable aggregates at $f_{HX} > 70\%$ because the PtBA block was soluble regardless of the CF/HX composition. The PS−P(CEMA-A) aggregates crashed out of the solvent phase at $f_{HX} = 73.3\%$ because the PS block became insoluble around this f_{HX}.

The observation that the d_h value rose, peaked, and then decreased for the PtBA−P(CEMA-T) aggregates before stabilization was intriguing. We initially associated these processes with the formation of swollen spherical micelles and then the deswelling of the micelles. On reflection, this interpretation was unreasonable. First, it was difficult to justify a d_h value of 240 nm for spherical micelles from such a diblock with $n_w = 305$ and $m_w = 95$ because the fully stretched diblock chains were shorter than 240 nm. Second, if the entire sample did participate in micelle formation at $f_{HX} = 56\%$, this solution should scatter more light than a solution at $f_{HX} = 75\%$ for the larger particles in the former solution. Also shown in Figure 1 are the scattered light intensity I_s of the samples as a function of f_{HX}. More light was scattered from the solution at $f_{HX} = 75\%$ than at $f_{HX} = 56\%$.

Such block aggregation behavior has been observed before. According to the literature, the initial d_h value increase could be attributed to "anomalous micellization".[1,41] It was only at the second stage of a sharp I_s increase at $f_{HX} \approx 62\%$ that the normal micelles were formed. Anomalous micellization occurred because of the chemical heterogeneity of the block copolymer samples. In this case, the anomalous micelles started to form at a low f_{HX} value of ~45% for the presence of a small fraction of PtBA−P(CEMA-T) chains that possessed n/m values that were significantly less than the average value of 3.2 as determined from NMR. This portion of the block copolymer formed micelle with morphologies that could be cylinders or others exhibiting large d_h values. As f_{HX} increased and the main portion of the diblock started to form micelles, the anomalous micelles disintegrated and their constituent chains comicellized with the other chains.

One may also plausibly argue that a trace amount of P(CEMA-T) homopolymer was the culprit for anomalous micellization. We tend to discount this argument, as the precursor to PtBA−P(CEMA-T) was prepared by anionic polymerization. For a "living" anionic polymerization, it is hard to imagine how homopolymer of the second block can be produced.

A comparison between the trends of d_h and I_s variation with f_{HX} for the PS−P(CEMA-A) sample suggests that anomalous micellization occurred for this diblock as well between $f_{HX} \approx 48\%$ and $f_{HX} \approx 62\%$. Since the maximum d_h value at $f_{HX} = 56\%$ is only 65 nm for this sample, we speculate that the anomalous micelles might be spherical in shape in this case.

DLS Study of Associated PtBA−P(CEMA-T) and PS−P(CEMA-A) Chains. Two protocols were used to add HX to CF solutions of the associated PtBA−P(CEMA-T) and PS−P(CEMA-A) chains. In protocol 1, HX addition was completed within fractions of a second. In protocol 2, HX was added at a controlled speed of 0.07 mL/min by a pump. Figure 2 compares the d_h and K_1^2/K_2 values of samples prepared from the two sample preparation protocols at various f_{HX} values. The reported data were determined 10 min after HX addition.

Regardless of the HX addition protocols, the d_h and K_1^2/K_2 variation trends could be divided into four regions. In region 1 between $f_{HX} \approx 45\%$ and $f_{HX} \approx 62\%$, small aggregates with high K_1^2/K_2 values were obtained. In region 2 between $f_{HX} \approx 62\%$ and $f_{HX} \approx 72\%$, K_1^2/K_2 decreased and d_h increased. Data from the two sample preparation protocols agreed with one another in regions 1 and 2. Region 3 was centered at $f_{HX} \approx 75\%$ where PS just started to collapse from the solvent phase. This region was characterized by large d_h and K_1^2/K_2 values as well as by rapid increase in the d_h values with time after HX addition. Figure 3 depicts how the d_h values changed with time for

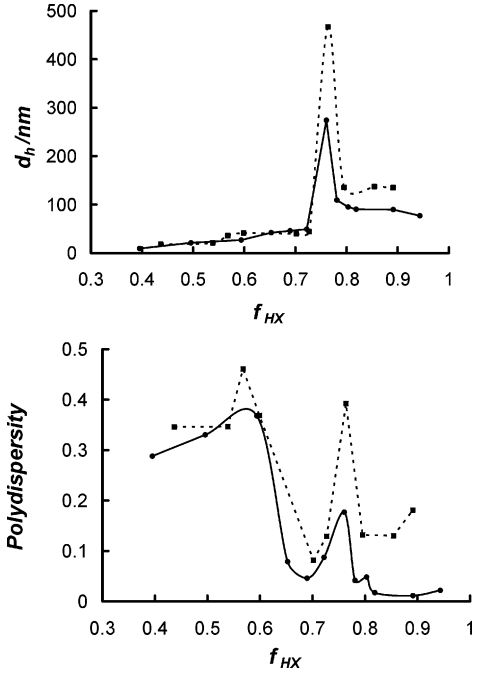

Figure 2. Variation in the d_h and K_1^2/K_2 values of the associating diblocks in CF/HX as a function of f_{HX} when HX was added by the fast (●) and slow (■) addition protocols.

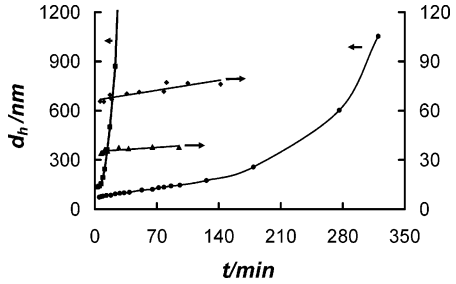

Figure 3. Variation in the d_h values of aggregates of the associating diblocks in CF/HX prepared by protocol 1 at $f_{HX} = 72\%$ (▲), $f_{HX} = 76\%$ (■), $f_{HX} = 78\%$ (●), and $f_{HX} = 80\%$ (◆) as a function of time.

samples prepared using protocol 1 at $f_{HX} = 72\%$, $f_{HX} = 76\%$, $f_{HX} = 78\%$, and $f_{HX} = 80\%$. While the aggregates at $f_{HX} = 72\%$ and $f_{HX} = 80\%$ were reasonably stable, the stability of the aggregates at 78% decreased, and the aggregates at $f_{HX} = 76\%$ were the least stable. Our visual inspection indicated that the aggregates at $f_{HX} = 76\%$ precipitated out from the solvent phase ~1 h after HX addition. In region 4 with $f_{HX} > 80\%$, both the d_h and K_1^2/K_2 values once again decreased, and the d_h values were larger than those in region 2. Comparing the two sample preparation protocols, we find that both the d_h and K_1^2/K_2 values were substantially larger for samples prepared from protocol 2 than those from protocol 1 in regions 3 and 4.

Region 1. The individual diblocks underwent anomalous micellization in this region with f_{HX} between 45% and 62%. This is in sharp contrast to the data of Figure 2 where a lacking of large particles was observed. Suspecting that the different DLS sample preparation methods used affected the results, we repeated the DLS experiment for the associated diblocks following the method used to obtain the data of Figure 1, which involved the addition of HX in aliquots, and then DLS measurement after each HX aliquot was injected in rapidly. This again failed to produce large particles between $f_{HX} \approx 45\%$ and $f_{HX} \approx 60\%$. On the basis of these observations, we conclude that H-bonding between the diblocks resulted in the shielding

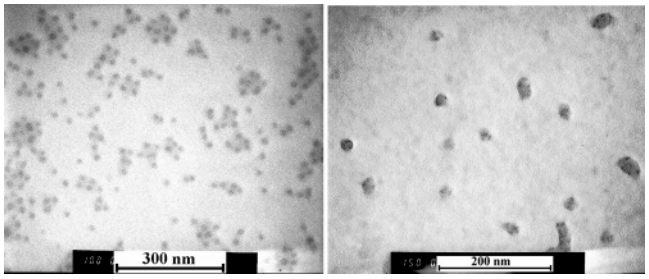

Figure 4. TEM images of aggregates of the associating diblocks prepared at $f_{HX} = 66\%$. The sample shown in the left panel was stained by OsO_4. The sample shown in the right panel was stained by $UO_2(Ac)_2$.

of the PCEMA blocks by both PtBA and PCEMA, and the better PCEMA shielding inhibited anomalous micellization.

Region 2. Normal micellization occurred in this region with f_{HX} approximately between 62% and 72% for the individual diblocks due to the collapsing of P(CEMA-T) and P(CEMA-A) from the solvent phase. Associated P(CEMA-T) and P(CEMA-A) seem to form also well-defined aggregates in this region as judged the low K_1^2/K_2 values observed (Figure 2). At $f_{HX} \approx 65\%$, the d_h values of the aggregates prepared from protocols 1 and 2 are similar at ~42 nm.

The left panel of Figure 4 shows a TEM image of aggregates prepared by protocol 1 at $f_{HX} = 66\%$. Since the sample was stained by OsO_4, only the double-bond-bearing PCEMA block is visible here. The spherical shape of the PCEMA domain is evident here. Averaging over 127 particles, we obtained $d_{TEM} = 17.3 \pm 1.3$ nm. Similar images were obtained for aggregates prepared from protocol 2.

The fact that the aggregates prepared from protocols 1 and 2 are essentially identical on the basis of our DLS and TEM results suggests that the aggregates formed in this region were preparation path independent and might be the thermodynamically controlled products or micelles. That the TEM diameter of the micelles is substantially smaller than $d_h \approx 42$ nm determined from DLS is reasonable because TEM gave only the core size and DLS yielded the overall size of the aggregates. Furthermore, DLS measured the size of the particles in a solvent-swollen state and TEM determined the size of the dry particles.

The distribution of the intrinsically incompatible PS and PtBA chains in the corona of comicelles of PS−P(CEMA-A) and PtBA−P(CEMA-T) is an intriguingly interesting problem and has been recently addressed by Hu and Liu[36] for such micelles prepared in different solvent mixtures. Gohy et al.[42] have addressed such an issue in other polymer systems. On one hand, inherent incompatibility between the different corona polymers will drive their phase separation. On the other, the natural tendency for a system to acquire the maximum entropy strives for the uniform distribution of the corona chain. A compromise between these two and possibly other factors may lead to different surface chain distributions, which include the "patched", "Janus", and "random" distributions as discussed by Hoppenbrouwers et al.[43] To see how the PtBA and PS chains were distributed on the surfaces of the PCEMA core of aggregates produced at $f_{HX} = 66\%$ by TEM, we needed a selective staining agent for either the PS or PtBA chains. Our inability to find such an agent forced us to take a detour, which involved the cross-linking of PCEMA first to lock in the micellar structure, then the selective hydrolysis of PtBA to PAA, and last the staining of PAA by $UO_2(AC)_2$. For the cross-linking of the PCEMA cores, we anticipated that the positions of the surface chains would not have reshuffled significantly for the fact that the tethering point of a PtBA chain should not change much

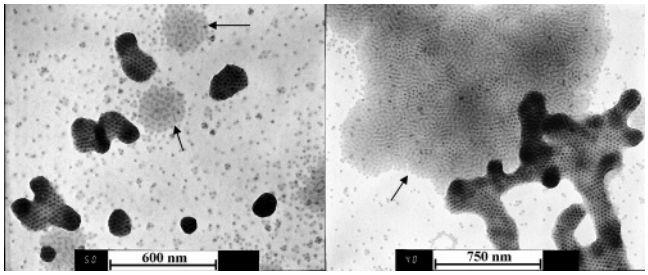

Figure 5. TEM images of aggregates of the associating diblocks prepared via protocol 1 at $f_{HX} = 75\%$ at $t = 17$ min (left) and $t = 60$ min (right).

with PtBA hydrolysis, and thus we could deduce at least approximately the original PtBA positions from the PAA positions. The right panel of Figure 4 shows a TEM image of a sample obtained after PCEMA cross-linking, PtBA hydrolysis, and PAA staining by $UO_2(AC)_2$. The PAA chains, which are supposed to look darker, definitely did not distribute uniformly on the surface of the PCEMA cores, as a uniform PAA layer on the PCEMA core surface would have produced dark TEM ring patterns.[36] Aside from this conclusion, we will not speculate further for the low quality of this image and others that we obtained.

Region 3. In region 3 centered around $f_{HX} = 75\%$, the PS chains just became insoluble in the solvent phase. This made the primary aggregates with mixed PtBA and PS corona chains unstable. The primary spherical aggregates underwent further aggregation to yield larger structures as suggested by our DLS data of Figure 3. This conclusion was confirmed by our TEM study of samples at $f_{HX} = 75\%$. Immediately after HX addition following protocol 1, we obtained TEM images similar to the one shown in the left panel of Figure 4 and confirmed thus the formation of spherical aggregates in the system. Figure 5 shows two TEM images of samples taken 17 and 60 min after HX addition. Some of the original aggregates had evidently undergone further assembly to form "superstructures" during the time intervals. As time progressed, the superstructures got bigger at the cost of the primary aggregates.

Seen in the thinner superstructure marked by an arrow in the right image of Figure 5 is a mixture of dark circles and dark worms. The circles are darker than the PCEMA cores of the individual primary aggregates seen scattered around the superstructures. This and the observation of many dark worms in the superstructures suggest that the dark circles might be projections of standing cylinders. Thus, the thinner superstructures consisted in the center region of cylindrical aggregates of the associated diblock chains. Since the TEM images of Figure 5 are in the electronic digital form, we have been able to make a closer examination of the darker or thicker superstructures in these images at higher magnifications and using different contrast. This revealed the presence of in-plane cylinders in some of the darker regions of these superstructures as well. Thus, the thicker superstructures may also consist of cylindrical aggregates packed with a higher degree of hexagonal order. Without confirmation by other techniques, it has been, however, difficult to conclude this without ambiguity. Regardless, what we can conclude definitely is that the superstructures did not derive directly from the physical laying together of the primary spherical aggregates. Instead, the primary aggregates had mutated and fused to yield the superstructures.

The formation of superstructures from the fusion of diblock aggregates or micelles in block-selective solvents has long been known. Eisenberg and co-workers[44] have, for example, observed

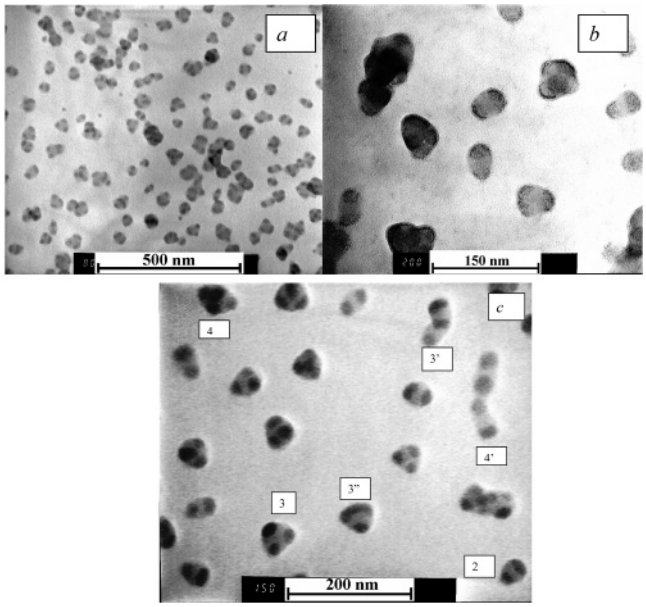

Figure 6. TEM images of aggregates of the associating diblocks prepared by the fast HX addition protocol. Images *a* and *c* were obtained by staining the specimens with OsO_4, and image *b* was obtained by specimen staining using $UO_2(Ac)_2$.

the fusion into microparticles containing hexagonally packed loops from PS−PAA vesicles in DMF (common solvent) and water (block-selective solvent for PAA) containing 6 vol % of water by adding NaCl. We observed the gradual fusion of core−shell PS−PCEMA spherical particles in tetrahydrofuran (common solvent) and acetonitrile (precipitant for PS and a marginal or approximately Θ solvent for PCEMA) with relatively low acetonitrile contents into composite particles containing hexagonally packed cylinders.[31] Some common features of these systems are that the original aggregates were only metastable and that the chains in the original aggregates possessed mobility. The spherical particles were only metastable in the present system because the solvent mixture had just turned poor for PS. PS chains and possibly PCEMA chains still possessed mobility because the HX content was still low. The driving force for the morphology transition in the case of Eisenberg and coworkers was the addition of NaCl. The chains were still mobile in the system because water content was low at 6%. The cause for metastability in the PS−PCEMA system was that acetonitrile was only a marginal solvent for PCEMA. The mobility of chains in the system was ensured by using a sufficiently low, e.g. 80%, acetonitrile content.

Region 4. In region 4 with $f_{HX} > 80\%$, the aggregates are bigger, as judged from data of Figures 2 and 3, than those in region 2 and are stable once again. Figure 6 shows TEM images of aggregates formed at $f_{HX} = 90\%$ prepared by the fast HX addition protocol. Image *a* suggests that the aggregates are monodisperse in size in agreement with the DLS K_2/K_1^2 result of Figure 2. The higher magnification image *c* offers a closer view of the particles. Most of the particles bear close resemblance to "molecules" that are built from commercial space-filling molecular models. The OsO_4-stained PCEMA domains in these "molecules" or "clusters" seem to adopt the shape of a hemispherical cap. On the basis of the insolubility of PS and the solubility of PtBA in this solvent composition region, PS should be concentrated in the interstitial space between the PCEMA-rich domains and PtBA should be grafted on the surfaces of the PCEMA domains. To confirm the location of the PtBA chains, we hydrolyzed the PtBA chains selectively to

facilitate their staining by $UO_2(Ac)_2$. To ensure the structural integrity or partial integrity of the clusters during PtBA hydrolysis or in the aspirating solvent DMF, we first irradiated the samples to cross-link the PCEMA domains. Figure 6b shows a TEM image of such a sample after PCEMA cross-linking, selective PtBA hydrolysis, and PAA staining. We note, first, the clusters of Figure 6b bear close structural resemblance to those in Figure 6a,c. This suggests that the clusters did not disintegrate in CH_2Cl_2 containing trifloroacetic acid, which was used to hydrolyze PtBA, or DMF, which was used to aspirate the hydrolyzed clusters. Since both CH_2Cl_2 and DMF are good solvents for PS, the retention of the integrity of the clusters in such solvents suggests that the phase separation between PS and PCEMA was not clean. Second, the PAA chains are located dominantly indeed on the surfaces of the PCEMA-rich hemispherical domains, as expected.

The clusters prepared in region 4 can take various shapes and consist of dimers, trimers, tetramers, etc. The trimers can be approximately triangular in shape (as marked by 3 in one case in Figure 6c) or be a bent rod (marked by 3′). Similarly, a tetramer can assume the shape of a tetrahedral (4) or a bent rod (4′). Further, two different PCEMA domains in a trimer can be fused as is found for the cluster labeled by 3″.

The formation mechanism, e.g., via a two-step mechanism involving first the formation of the primary aggregates and then the fusion of the small aggregates or via some kind of concerted mechanism, and the origin, kinetic vs thermodynamic, of "molecular-model-like" nanoclusters can be intriguing and interesting. These are, however, questions not readily answered. What we want to emphasize here is that the structures seen here are new on the basis of self-assembly of block copolymers in block-selective solvents. Indeed, there have been quite some reports on the morphologies of triblock copolymers. Most of the observed aggregates had the core−shell−corona spherical[45−51] or cylindrical[7,52−55] morphologies. Occasionally, aggregates with surface-segregated chains have been reported from linear triblocks but no patterns like what is seen here.[43] The closet relative that we could find for the structures reported here are the multicompartment micelles of B−C−D miktoarm triblocks reported by the groups of Lodge and Hillmyer.[56] Aside from self-assembly, microclusters of similar shapes have been prepared by the group of Pine[57] via the fusion of premade polymer spheres by an emulsion process. We have recently reported the preparation of bumpy and chain-segregated nanospheres via a one-pot emulsion process from the use of two diblock surfactants.[58]

We have also studied the samples prepared by the slow HX addition protocol. The particles prepared by the fast HX addition protocol are on the average smaller and more monodisperse (Figure 2). This is reasonable because the samples prepared by the slow HX addition protocol would have spent more time in region 3, where the aggregates were instable and underwent further self-assembly and growth in size.

IV. Conclusions

The coaggregation of PS−P(CEMA-A) and PtBA−P(CEMA-T) in CF/HX mixtures with different f_{HX} contents has been examined. In contrast to the individual diblocks, the diblock mixtures did not undergo significant anomalous micellization in CF/HX in composition region 1 with f_{HX} between 45% and 62%. This was caused most likely by the better shielding of the PCEMA blocks by both the PtBA and PCEMA chains in the associated state of the diblocks and thus the reduced tendency for the different PCEMA chains to aggregate at such low f_{HX} values. In region 2 with f_{HX} between ~62% and ~72%, spherical micelles were formed with PCEMA making up the core and with PtBA and PS making up the corona. The distribution of the PtBA chains in the corona was nonuniform and probably patched. In region 3 in the neighborhood of $f_{HX} \approx 75\%$ when the PS block just became insoluble, the spherical primary aggregates were instable. They underwent further self-assembly to yield superstructures sometimes with crystal-like internally ordered cylindrical PCEMA domains. The coaggregates became stable once again in region 4 with $f_{HX} > \sim 80\%$. In this region, the coaggregates formed bore much structural resemblance to molecular models. In such an aggregate, the hemispherically shaped PCEMA-rich domains were glued together by a central PS-rich domain. Grafted onto the surfaces of the PCEMA domains were the soluble PtBA chains to render the aggregates dispersibility in solvents.

Acknowledgment. The Special Research Opportunity Program of the Natural Sciences and Engineering Research Council of Canada is gratefully acknowledged for financial support.

References and Notes

(1) Tuzar, Z.; Kratochvil, P. *Surf. Colloid Sci.* **1993**, *15*, 1.
(2) Forster, S.; Antonietti, M. *Adv. Mater.* **1998**, *10*, 195.
(3) Canham, P. A.; Lally, T. P.; Price, C.; Stubbersfield, R. B. *J. Chem. Soc., Faraday Trans.* **1980**, *76*, 1857.
(4) Zhang, L. F.; Eisenberg, A. *Science* **1995**, *268*, 1728.
(5) Ding, J. F.; Liu, G. J.; Yang, M. L. *Polymer* **1997**, *38*, 5497.
(6) Yu, K.; Eisenberg, A. *Macromolecules* **1998**, *31*, 3509.
(7) Stewart, S.; Liu, G. *Angew. Chem., Int. Ed.* **2000**, *39*, 340.
(8) Raez, J.; Barjovanu, R.; Massey, J. A.; Winnik, M. A.; Manners, I. *Angew. Chem., In. Ed.* **2000**, *39*, 3862.
(9) Frankowski, D. J.; Raez, J.; Manners, I.; Winnik, M. A.; Khan, S. A.; Spontak, R. J. *Langmuir* **2004**, *20*, 9304.
(10) Grumelard, J.; Taubert, A.; Meier, W. *Chem. Commun.* **2004**, 1462.
(11) Jenekhe, S. A.; Chen, X. L. *Science* **1999**, *283*, 372.
(12) Ding, J. F.; Liu, G. J. *Macromolecules* **1997**, *30*, 655.
(13) Opsteen, J. A.; Cornelissen, J.; van Hest, J. C. M. *Pure Appl. Chem.* **2004**, *76*, 1309.
(14) Checot, F.; Lecommandoux, S.; Gnanou, Y.; Klok, H. A. *Angew. Chem., In. Ed.* **2002**, *41*, 1339.
(15) Pochan, D. J.; Chen, Z. Y.; Cui, H. G.; Hales, K.; Qi, K.; Wooley, K. L. *Science* **2004**, *306*, 94.
(16) Zhu, J. T.; Liao, Y. G.; Jiang, W. *Langmuir* **2004**, *20*, 3809.
(17) Cameron, N. S.; Corbierre, M. K.; Eisenberg, A. *Can. J. Chem.* **1999**, *77*, 1311.
(18) Liu, G.; Yan, X.; Li, Z.; Zhou, J.; Duncan, S. *J. Am. Chem. Soc.* **2003**, *125*, 14039.
(19) Yan, X.; Liu, G.; Li, Z. *J. Am. Chem. Soc.* **2004**, *126*, 10059.
(20) Massey, J. A.; Winnik, M. A.; Manners, I.; Chan, V. Z. H.; Ostermann, J. M.; Enchelmaier, R.; Spatz, J. P.; Moller, M. *J. Am. Chem. Soc.* **2001**, *123*, 3147.
(21) Park, M.; Harrison, C.; Chaikin, P. M.; Register, R. A.; Adamson, D. H. *Science* **1997**, *276*, 1401.
(22) Thurn-Albrecht, T.; Schotter, J.; Kastle, C. A.; Emley, N.; Shibauchi, T.; Krusin-Elbaum, L.; Guarini, K.; Black, C. T.; Tuominen, M. T.; Russell, T. P. *Science* **2000**, *290*, 2126.
(23) Li, Z.; Zhao, W.; Liu, Y.; Rafailovich, M. H.; Sokolov, J.; Khougaz, K.; Eisenberg, A.; Lennox, R. B.; Krausch, G. *J. Am. Chem. Soc.* **1996**, *118*, 10892.
(24) Silva, G. A.; Czeisler, C.; Niece, K. L.; Beniash, E.; Harrington, D. A.; Kessler, J. A.; Stupp, S. I. *Science* **2004**, *303*, 1352.
(25) Stupp, S. I. *MRS Bull.* **2005**, *30*, 546.
(26) Vriezema, D. M.; Aragones, M. C.; Elemans, J.; Cornelissen, J.; Rowan, A. E.; Nolte, R. J. M. *Chem. Rev.* **2005**, *105*, 1445.
(27) Kataoka, K.; Harada, A.; Nagasaki, Y. *Adv. Drug Deliv. Rev.* **2001**, *47*, 113.
(28) Chen, D. Y.; Jiang, M. *Acc. Chem. Res.* **2005**, *38*, 494.
(29) Zhao, H. Y.; Liu, S. Y.; Jiang, M.; Yuan, X. F.; An, Y. L.; Liu, L. *Polymer* **2000**, *41*, 2705.
(30) Duan, H. W.; Chen, D. Y.; Jiang, M.; Gan, W. J.; Li, S. J.; Wang, M.; Gong, J. *J. Am. Chem. Soc.* **2001**, *123*, 12097.
(31) Ding, J. F.; Liu, G. J. *Macromolecules* **1999**, *32*, 8413.
(32) Berne, B. J.; Pecora, R. *Dynamic Light Scattering with Applications to Chemistry, Biology, and Physics*; Dover Publications: Mineola, NY, 1976.

(33) Brandrup, J.; Immergut, E. H. *Polymer Handbook*, 3rd ed.; John Wiley & Sons: New York, 1989.
(34) Guo, A.; Liu, G. J.; Tao, J. *Macromolecules* **1996**, *29*, 2487.
(35) Lu, Z. H.; Liu, G. J.; Duncan, S. *Macromolecules* **2004**, *37*, 174.
(36) Hu, J. W.; Liu, G. J. *Macromolecules* **2005**, *38*, 8058.
(37) Askew, B.; Ballester, P.; Buhr, C.; Jeong, K. S.; Jones, S.; Parris, K.; Williams, K.; Rebek, J. *J. Am. Chem. Soc.* **1989**, *111*, 1082.
(38) Zhou, J. Y.; Li, Z.; Liu, G. J. *Macromolecules* **2002**, *35*, 3690.
(39) Liu, G. J.; Zhou, J. Y. *Macromolecules* **2003**, *36*, 5279.
(40) Liu, G. J.; Zhou, J. Y. *Macromolecules* **2002**, *35*, 8167.
(41) Zhou, Z. K.; Chu, B. *Macromolecules* **1988**, *21*, 2548.
(42) Gohy, J. F.; Khousakoun, E.; Willet, N.; Varshney, S. K.; Jerome, R. *Macromol. Rapid Commun.* **2004**, *25*, 1536.
(43) Hoppenbrouwers, E.; Li, Z.; Liu, G. J. *Macromolecules* **2003**, *36*, 876.
(44) Zhang, L. F.; Bartels, C.; Yu, Y. S.; Shen, H. W.; Eisenberg, A. *Phys. Rev. Lett.* **1997**, *79*, 5034.
(45) Stewart, S.; Liu, G. J. *Chem. Mater.* **1999**, *11*, 1048.
(46) Kriz, J.; Masar, B.; Plestil, J.; Tuzar, Z.; Pospisil, H.; Doskocilova, D. *Macromolecules* **1998**, *31*, 41.
(47) Yu, G. E.; Eisenberg, A. *Macromolecules* **1998**, *31*, 5546.
(48) Talingting, M. R.; Munk, P.; Webber, S. E.; Tuzar, Z. *Macromolecules* **1999**, *32*, 1593.
(49) Lambert, O.; Reutenauer, S.; Hurtrez, G.; Dumas, P. *Macromol. Symp.* **2000**, *161*, 97.
(50) Ishizone, T.; Sugiyama, K.; Sakano, Y.; Mori, H.; Hirao, A.; Nakahama, S. *Polym. J.* **1999**, *31*, 983.
(51) Zhou, Z. L.; Li, Z. B.; Ren, Y.; Hillmyer, M. A.; Lodge, T. P. *J. Am. Chem. Soc.* **2003**, *125*, 10182.
(52) Lei, L. C.; Gohy, J. F.; Willet, N.; Zhang, J. X.; Varshney, S.; Jerome, R. *Macromolecules* **2004**, *37*, 1089.
(53) Yan, X. H.; Liu, G. J.; Liu, F. T.; Tang, B. Z.; Peng, H.; Pakhomov, A. B.; Wong, C. Y. *Angew. Chem., In. Ed.* **2001**, *40*, 3593.
(54) Li, Z.; Liu, G. J. *Langmuir* **2003**, *19*, 10480.
(55) Yan, X. H.; Liu, G. J.; Haeussler, M.; Tang, B. Z. *Chem. Mater.*, in press.
(56) Li, Z. B.; Kesselman, E.; Talmon, Y.; Hillmyer, M. A.; Lodge, T. P. *Science* **2004**, *306*, 98.
(57) Manoharan, V. N.; Elsesser, M. T.; Pine, D. J. *Science* **2003**, *301*, 483.
(58) Zheng, R. H.; Liu, G. J.; Yan, X. H. *J. Am. Chem. Soc.* **2005**, *127*, 15358.

MA052435I